PHYSICAL REVIEW B VOLUME 19, NUMBER 4 15 FEBRUARY 1979

Characterization of amorphous semiconducting silicon-boron alloys prepared by plasma decomposition

C. C. Tsai *

Department of Physics and the James Franck Institute, The University of Chicago, Chicago, Illinois 60637

(Received 22 September 1978)

Amorphous semiconducting films of the Si-B binary system have been prepared by rf plasma decomposition of silane-diborane gas mixtures. The infrared vibrational modes, optical absorption, conductivity, spin resonance, and hydrogen content of these films have been studied as a function of preparation conditions. These alloy films differ substantially from chalcogenide glasses on the one hand and from group-IV amorphous semiconductors on the other. They contain between 10- and 45-at.% hydrogen and between 10^{18} and 10^{19} cm^{-3} unpaired spins. The spin-resonance linewidth is inhomogeneously broadened because of a large spectrum of bond distances and bond strengths. This spectrum yields a few very broad infrared absorption bands and, in the boron-rich films, an unusually broad and slowly varying absorption edge. This large spectrum of bond strengths results from the electron-deficient nature of boron which can associate with the environment in two-center and three-center bonds involving hydrogen, silicon, and other boron atoms. The slope of the conductivity curves decreases slowly without distinct exponential regions and without showing Mott's law of variable-range hopping near 77 K. Except for the two end compositions of the binary system, the Fermi level is close to the valence band, presumably because tetrahedrally coordinated boron atoms act as acceptors and produce a self-doping effect.

I. INTRODUCTION

The preparation of amorphous Si by means of plasma decomposition of silane has attracted great interest lately because this method produced the first amorphous semiconductor which had a sufficiently low density of intrinsic defects so that controlled doping was possible.[1-7] Several papers reported the superior electronic properties of this material,[8-16] amorphous p-n junctions[17] were made, and quite efficient Schottky-barrier solar cells[18,19] were fabricated. At the present time plasma deposited amorphous silicon is one of the most thoroughly studied amorphous semiconductors.[20-30]

The plasma decomposition technique was used to prepare amorphous C,[31] Ge,[2] SiC,[32] GaP,[33] and As.[6] All these materials, except As, were quite unlike evaporated or sputtered films of the same materials. This is because hydrides are used for the plasma decomposition which introduces appreciable amounts of hydrogen[20,27,29,34,35] into these amorphous films.

This paper reports a detailed investigation of silicon-boron alloys prepared by plasma decomposition of gas mixtures containing silane, SiH_4, and diborane, B_2H_6. The infrared spectra are studied to gain some information about the structure and the ways hydrogen is incorporated. The composition was determined by Auger, flame spectroscopic analysis, and hydrogen effusion studies. The optical absorption near the fundamental absorption edge was measured to determine the optical gap as a function of alloy composition. Measurements of the conductivity between 77 and 450 K as well as of the paramagnetic resonance were carried out to further characterize the material as a function of alloy composition and preparation conditions.

II. PREPARATION

The advantage of glow-discharge plasma deposition is that chemical reactions can take place at relatively low ambient temperatures. This is because the electrons have energies of order 10 eV and thus are able to break molecular bonds. A variety of chemically active species may be present in the plasma, and the deposition of films on a substrate involves complex surface reactions of electrons, neutrals, and ion species. Film properties depend on surface conditions like substrate temperature and potential, for example, as well as on plasma conditions. The latter is influenced by a number of parameters such as power level, gas pressure, flow rate, pumping speed, and the geometry of the reaction chamber.

Two methods have been used to excite a radio-frequency (rf) discharge. The rf power can be coupled to the plasma either inductively or capacitively. The capacitive system, which was first used by Knights,[5] shows better reproducibility and can be enlarged more easily than the inductive system, which was originally used by Chittick *et al.*[36] After verifying that both systems produce similar films, we adopted the diode system. Figure 1 shows the layout of our reaction

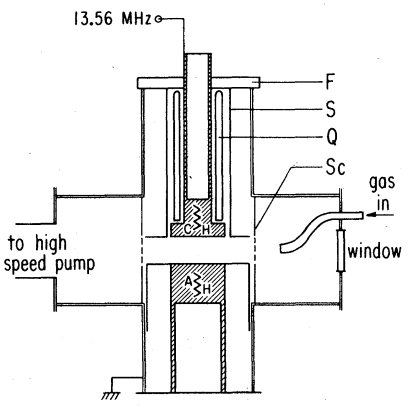

FIG. 1. Schematic sketch of plasma reactor consisting of 7.5-cm-diam stainless-steel cross. A = anode, C = cathode, F = ceramic flange, H = heater, Q = insulating quartz cylinder, Sc = grounded screen, S = grounded shield.

chamber.[30] Since electrons have much higher mobilities than ions do, and the two electrodes have different areas (the diameters of the anode and the cathode are 5.8 and 3.3 cm, respectively), the ungrounded electrode self-biases to a negative potential in the rf glow-discharge plasma. This dc bias is typically 100–200 V for a rf power of 5–15 W. Film properties depend on this substrate bias as well as the substrate temperature T_s. We therefore distinguish between films deposited onto a substrate on the cathode C, and the anode A, referring to the grounded electrode as the anode. Films deposited on the anode at T_s=25 and 270°C, and on the cathode at T_s=25 and 270°C will be denoted by $A(25)$, $A(270)$, $C(25)$, and $C(270)$, respectively. The present films are obtained by diluting the desired SiH_4-B_2H_6 mixture with argon at a 1:60 ratio, by using a low pressure of 0.15 Torr, a high flow rate of about 100 scc/min, a low 13.56-MHz power of 5–15 W, and a small separation of 1.2–2.4 cm between the capacitor plates. The deposition rate is about 2–10 Å/sec, with the lower rate corresponding to high substrate temperatures and/or large boron fractions. Typical film thickness ranges from 0.3 to 30 μm.

Various substrate materials were used for different purposes: Corning 7059 glass for transport, optical, and Auger measurements; aluminum foil for hydrogen-evolution experiments after removal of Al substrate by etching and chemical analysis; crystalline silicon wafers, KRS-5 (Ref. 37) and sapphire substrates for infrared transmission spectroscopy.

Since SiH_4 is highly flammable in air and B_2H_6 is extremely toxic, it is important to have a leak-tight system. Repeated evacuation and argon flushing of the reaction system are necessary before and after each deposition run. Moreover, the entire system was built under a hood for extra protection. The exhaust gases are first diluted with nitrogen, then thermally decomposed in an oven held at 800 °C, and finally passed through water and led to the outside.

Despite the reproducibility achieved with the control of the plasma conditions, one is not yet certain which conditions yield films with the most desirable properties. It is therefore not surprising that plasma deposited samples from different laboratories differ in their properties. However, one clearly wishes to promote surface reactions that lead to decomposition of hydrides while suppressing the gas-phase nucleation, which is likely to lead to polymerization and yield low-density and hydrogen-rich polymeric materials. Low pressure and small plate separation decrease the probability of collisions among species in the gas phase, and increase that of collisions of reactant species with substrate surface, thereby reducing the gas-phase nucleation and promoting surface reactions. Argon dilution avoids collisions among reactive species; low-power level and high flow rate lower the average energy density in the plasma and thereby suppress gas-phase reactions; high substrate temperature also enhances the surface reactions that lead to decomposition.

III. AUGER ANALYSIS

The relative efficiencies of depositing boron and silicon from the plasma of a SiH_4-B_2H_6 gas mixture determine the film composition. We determined the relative B and Si contents in our films by Auger spectroscopic analysis.[38] Figure 2 shows the Auger spectrum, representing the first derivative, $dn(E)/dE$, of the energy distribution function of the Auger electrons plotted against electron energy, of a film deposited on the cathode at 270 °C, $C(270)$, with a boron fraction in the gas phase, X_g, of 0.36, which is defined as

$$X_g=\frac{[B]}{[B]+[Si]}\bigg|_{Gas}=\frac{2N(B_2H_6)}{2N(B_2H_6)+N(SiH_4)}, \qquad (1)$$

where $N(B_2H_6)$ and $N(SiH_4)$ are the concentrations of B_2H_6 and SiH_4 in the gas mixture, respectively.

The Auger spectrum shows characteristic peaks of Si near 92 and 1619 eV and of B near 179 eV. The Ar peak near 215 eV arises mainly from the

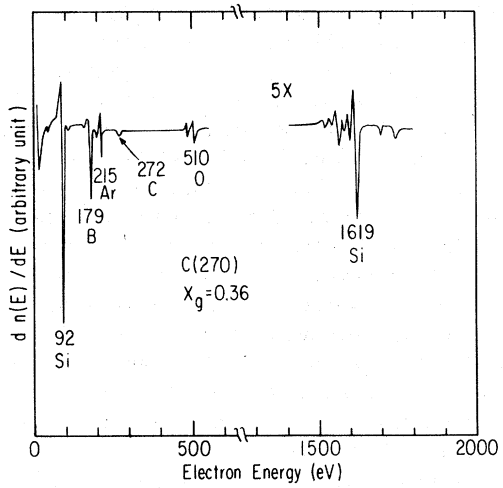

FIG. 2. Auger spectrum of a cathode film prepared at T_s = 270 °C with boron fraction X_g = 0.36 in the gas. The spectrum was taken with an electron beam energy of 3 keV, and a beam current of 1 μA. The energies at which Auger transitions occur for elements involved are given.

sputter etching used to remove the oxidized surface layer or to obtain a depth profile.

Sometimes traces of O with peaks near 510 eV and *C* with peaks near 272 eV are seen, especially near the top surface of films. The oxygen depth profile shown in Fig. 3 reveals a sharp decrease with increasing distance from the surface. After the first 50 Å, the oxygen level drops to less than 1 at. %. Generally, more oxygen and carbon are found in *A*(25) samples with high boron content. This will be discussed further in connection with the infrared studies below.

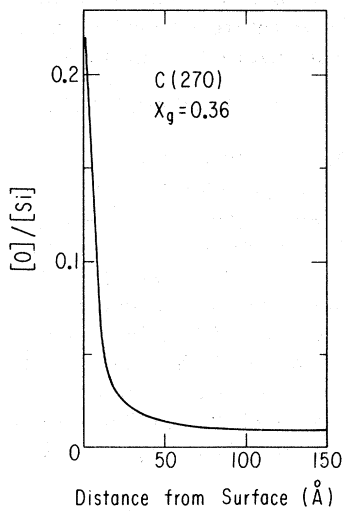

FIG. 3. Oxygen depth profile expressed as the ratio of oxygen to silicon concentrations vs the distance from the surface for a cathode film prepared at T_s = 270 °C with X_g = 0.36. The ratio of oxygen to silicon concentration was obtained from the ratio of the peak-to-peak height of the Auger transitions in oxygen at 510 eV to that in silicon at 1619 eV normalized by the relative sensitivity factors.

Because of the relatively low electrical conductivity of the samples, localized charging can occur on the specimen surface, which can cause a shift in the Auger peak energies and a change in the peak-to-peak amplitude of $dn(E)/dE$. Despite the deposition of a gold overlayer to facilitate discharging, noticeable charging can still occur in some high-resistivity samples. One way of detecting charging effects is to measure the ratio of the peak-to-peak amplitudes of the Si transition at 92 eV to that at 1619 eV because charging affects the Auger peaks more at low energies than at high energies. This ratio should be 5.4 according to measurements on boron-doped crystalline Si which had a high conductivity and thus no charging problems. In our amorphous films we found the ratio between 4 and 7. In order to reduce errors resulting from charging as much as possible, we selected the highest-energy Auger peaks, 179 eV for boron and 1619 eV for silicon. The B(179) peak seems to be less affected by surface charges than the Si(92) peak. This is fortunate because there are no higher-energy Auger transitions available for boron.

Determination of film composition was made by atomic absorption spectroscopic analysis on a standard sample prepared with a boron fraction X_g=0.24 in the gas.[39] The boron fractions in the film, X_f, of all samples were then obtained by comparing their B(179)/Si(1619) ratios with that of the standard, where X_f is defined as

$$X_f = \left.\frac{[B]}{[B]+[Si]}\right|_{\text{Film}} . \qquad (2)$$

An independent quantitative estimate can be obtained by normalizing the peak-to-peak heights of the Auger transitions with the appropriate relative elemental sensitivity factors.[40] This method yields X_f=0.17 for the standard sample compared to the value 0.19 obtained from atomic absorption spectroscopic analysis. Because of the charging effect, the error of the Auger analysis is about 2 at. %.

The depth profile indicates that apart from the surface layers, the film composition is uniform throughout the film thickness. The boron fraction in the film, X_f, is plotted against that in the

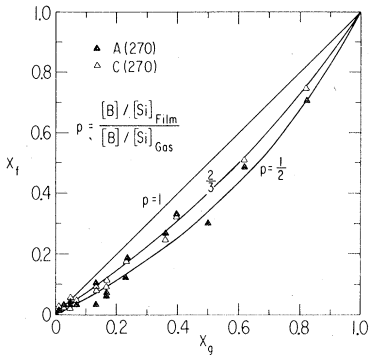

FIG. 4. Boron fraction in the film as a function of that in the gas for films prepared at T_s = 270 °C. The relative incorporation efficiency p of boron as compared to silicon is $p = 0.65 \pm 0.15$.

gas, X_g, in Fig. 4 for a number of films prepared on both the cathode and the anode at substrate temperature T_s = 270 °C. We find that the relative incorporation efficiency p of boron as compared to silicon is $p = 0.65 \pm 0.15$, quite independent of the substrate temperature, the potential, or the composition of gas. One therefore can conveniently prepare hydrogenated amorphous Si-B alloys with any composition in the binary system by properly choosing the concentration of the SiH_4-B_2H_6 gas mixture. In contrast, Spear and LeComber[2] reported a considerably smaller efficiency of boron incorporation at low B concentration. In the case of phosphorus doping, they found that the maximum number of phosphorus atoms that could be incorporated into the silicon is limited to a density of 3×10^{19} cm^{-3} in the film. We do not find such a limit in the Si-B system.

IV. HYDROGEN CONTENT

Substantial amounts of hydrogen of the order of 10–30 at.% are incorporated into a-Si films during the deposition.[20,27,29,34] This concentration far exceeds that of dangling bonds observed in vapor deposited a-Si (about 10^{20} cm^{-3}), and is sufficiently high to modify the amorphous network. We now know that these films owe their remarkable properties not so much to the plasma deposition technique, but to the incorporation of such large quantities of hydrogen, which greatly reduces the density of the localized gap states and makes doping possible.[1,2,7]

We found that the amorphous films obtained from the glow-discharge decomposition of SiH_4 + B_2H_6 gas mixtures also contain similarly high density of hydrogen, between 10 and 45 at.%. One therefore actually deals with hydrogenated amorphous silicon-boron alloys, to which we refer as a-Si-B-H.

Although conventional methods such as Auger spectroscopy and electron microprobe analysis are not sensitive for detecting hydrogen, the hydrogen content of these films can be determined in a rather simple way since hydrogen evolves as the material is heated. The amount of H_2 gas evolved can be obtained by measuring either the volume increase at a fixed pressure, or, more accurately, the pressure increase in a fixed volume as a known quantity of material is heated at a constant rate. We used a rate of 15 °C/min.

Mass spectroscopic analysis verified that the evolved gas is, indeed, predominantly hydrogen. The ratio of the number of hydrogen atoms to that of silicon and boron atoms is shown in Fig. 5 for a-Si-B-H films deposited at a substrate temperature of 270 °C with different boron fractions in the gas. It ranges from 0.10 to 0.42, which corresponds to a hydrogen content of 9–30 at.%, depending on the substrate potential and the boron fraction. On the silicon-rich side of the alloy system, films deposited on either electrode contain similar amounts of hydrogen. With increasing boron concentration, the hydrogen content of the anode films rises rapidly, while that of the cathode films decreases slightly. The effect of the substrate potential is therefore substantially enhanced on the boron-rich side, where anode films contain up to three times more hydrogen than the cathode films. It is interesting to note that the efficiency of boron incorporation is independent of bias, but the hydrogen content depends on bias. Therefore, it seems that for the boron-rich alloys the substrate bias determines the dissociation of hydrogen from the boron-hydride

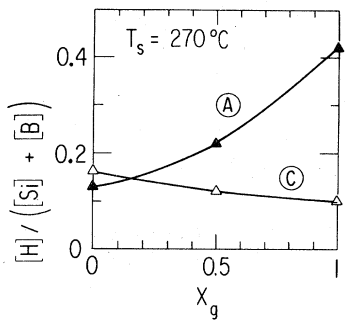

FIG. 5. Ratio of the hydrogen concentration to that of silicon and boron as a function of boron fraction in the gas for films deposited at T_s = 270 °C.

species on the substrates during film deposition. The detailed role played by the substrate potential in the plasma decomposition of hydrides to yield amorphous films is not understood and needs further study.

The substrate temperature T_s during deposition is another factor that determines the hydrogen level. Materials deposited at T_s=25 °C have 17–45 at.% hydrogen, with the higher value again corresponding to larger boron concentrations.

The substrate bias as well as temperature not only affects the hydrogen content of the films, but also determines the ways in which hydrogen is incorporated. In the case of hydrogenated silicon,[30] all anode films have short-chain polysilane units $(SiH_2)_n$, whereas the cathode films do not. Anode samples have predominantly polysilane chain segments at T_s=25 °C, but at higher substrate temperatures most of their hydrogen is bonded as monohydride units with small fractions bonded as isolated dihydride units and polysilane chain segments. Cathode samples, on the other hand, have predominantly isolated monohydride units with small fractions of isolated dihydride units, regardless of T_s.

The evolution of hydrogen from the a-Si-B-H alloys, with a heating rate of 15 °C/min, occurs near 350 °C for T_s=25 °C samples, and near 550 °C for T_s=270 °C samples.

A small amount of argon was found in the cathode samples on the silicon-rich side of the a-Si-B-H alloys. For T_s = 270 °C, the argon content decreases with increasing boron concentration: It is about 3 at.% for the hydrogenated silicon with X_g=0, drops to below 1 at.% at X_g=0.5, and is below the detection limit of 10^{-3} at.% at X_g=1.0, which corresponds to hydrogenated boron. It is surprising that the argon concentration increases with the substrate temperature. In contrast, the amount of argon observed in the anode samples was always less than the detection limit of 10^{-3} at.%. These results are quite plausible; after all, the glow discharge is sustained mainly by argon, which makes up 98% of the gases in the reaction chamber. Having a negative potential of 100–200 V, the cathode is subjected to a constant bombardment of Ar^+ ions, some of which are then trapped in the cathode films.

V. INFRARED ABSORPTION, BONDING, AND STRUCTURE

Since boron and hydrogen are difficult to study by the x-ray technique, infrared spectroscopy was used to investigate the structure and bonding of the a-Si-B-H alloys.

A. A(25) samples

The incorporated hydrogen is bonded to silicon or boron. This can be seen in the infrared transmission spectra.[41] Typical film thickness ranges from 5 to 30 μm. The transmission spectra of A(25) films on KRS-5 substrates are shown in Fig. 6 as a function of X_g, the boron content in the gas. The wave-number scale changes at 2000 cm^{-1} because of a grating change in the spectrometer. Since films with somewhat different thicknesses are involved, only relative comparisons of the absorption strengths should be made. With increasing boron concentration in the film, the absorption near 2560 cm^{-1} due to B-H stretching vibrations[42] grows, while that near 2000–2100 cm^{-1} due to the Si-H stretching vibrations[22,25,30] drops proportionally. In the hydrogenated boron sample with X_g=1, a broader band near 2000 cm^{-1} is observed. Its origin, which is of course not related to silicon, will be discussed later. Another feature which grows with increasing boron content is a broad absorption band extending from 1100 to 400 cm^{-1}, which is superimposed on the deformation modes of the Si-H bonds near 650, 840, and 890 cm^{-1}.[22,25,30] This broad feature, also observed by Blum *et al.*[42] between 1000 and 800 cm^{-1} and by Berezin *et al.*[43] between 800 and 550 cm^{-1} in evaporated amorphous boron films, arises from B-B bonds.

This broad feature appears to be missing for the X_g=1 sample. However, this film was difficult to measure because of its great reactivity with moisture. As a consequence, the pure boron films require further investigation. The breakdown of the k-selection rule in amorphous solids,

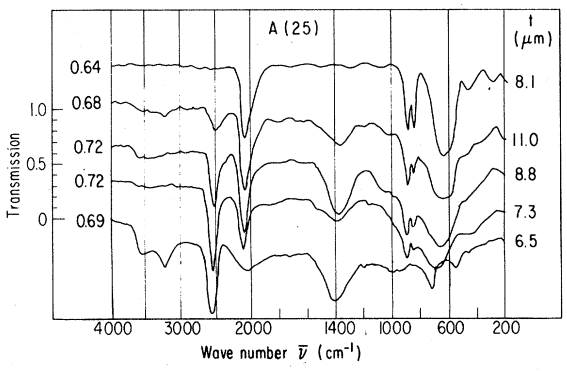

FIG. 6. Infrared absorption spectrum of anode films prepared at T_s=25 °C with boron fractions X_g=0, 0.25, 0.5, 0.75, and 1, respectively, in the gas. The film thickness and the transmission measured at $\bar{\nu}$=4000 cm^{-1} are given for each curve.

caused by the absence of long-ranged order, allows to some extent the infrared activity of all vibrational modes. As a consequence, the infrared absorption lacks the sharp features observed in the lattice vibrations of the corresponding crystals. Whatever structure might remain is diminished by structural dispersion, such as a variation in bond length and bond angle. Moreover, it is well known that boron forms three-center covalent bonds.[44] This is because boron has only three valence electrons, while there are four valence orbitals, $2s$, $2p_x$, $2p_y$, and $2p_z$. Since more atomic orbitals are available for chemical bonding than electrons, boron is "electron deficient" in the classical sense. As a result, three boron atoms can share two electrons and form a three-center bond. Such a three-center two-electron bond is an extension of the ordinary two-center two-electron bond, and is found in a large number of boron compounds whenever three atomic orbitals, each associated with different atoms, can be combined to give a single lowest-energy molecular orbital. The three atomic orbitals can form either one bonding and two antibonding molecular orbitals, or one bonding, one nonbonding, and one antibonding molecular orbital. With increasing boron fraction in the a-Si-B-H alloys, the probability increases for three boron atoms to get close enough to form a three-center bond. However, the bond lengths cannot have their optimal value because the position of each of the atoms is also conditioned by its other bonds to the network. As a consequence, it is likely that such three-center bonds have rather large variation in their strengths. This is probably the main cause for the broadening of the infrared absorption bands attributed to B-B vibrations.

The third effect of boron on the infrared transmission spectra is the appearance of an absorption band near 1350 cm^{-1}. This had been identified as due to B-O vibrations. It was also observed in evaporated amorphous boron films by Zimmerman III *et al.*[45] and Blum *et al.*[42] Only those $A(25)$ films which contain appreciable boron concentrations exhibit this B-O absorption band. Figure 7 shows as an example the progressive oxidation of an anode film with $X_g=0.75$. Curve 1 was obtained after the sample was exposed to room air having 30% relative humidity for half an hour. Substantial oxidation of boron had already taken place. Exposure to room air for two additional hours, as seen in curve 2, revealed further growth of the B-O band near 1350 cm^{-1}. At this point the sample was stored in dry argon, the oxidation processes stopped immediately, and after 42 h the same transmission spectrum as shown by curve 2 was obtained. This leaves no doubt that this absorption band is associated with oxides. As soon as the film was exposed to air again, the absorption band continued to grow. Curves 3 and 4 of Fig. 7 were taken after the sample remained in room air for another 18 h and 7 days, respectively. Also observed in curve 4 was the development of a Si-O band near 1050 cm^{-1}. This study indicates that oxidation occurred after preparation, although small amounts of contamination during deposition cannot be ruled out.

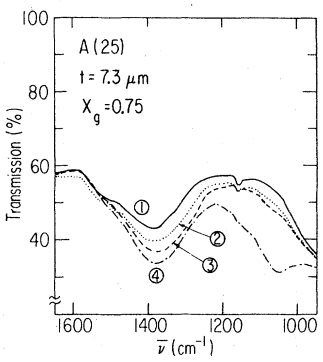

FIG. 7. Progressive oxidation of a 7.3-μm anode film deposited at $T_s=25$ °C. Curve 1 was obtained after the sample was exposed to room air having 30% relative humidity for 0.5 h. Exposure to room air for two additional hours, as well as subsequent storage in dry argon for 42 h resulted in curve 2. Curves 3 and 4 were taken after the sample remained in room air for another 18 h and 7 days, respectively.

That $A(25)$ samples with high boron content are very porous can also be seen from the presence of infrared absorption bands near 1150 cm^{-1} (Fig. 7) and 3200–3500 cm^{-1} (Fig. 6), corresponding to B-C[42] and O-H[45] vibrations, respectively, in addition to the B-O and Si-O absorption bands. In contrast, the corresponding cathode films and all the high T_s samples are not porous and show no evidence of oxygen or carbon contamination in the infrared spectra. Although all films have substantial amounts of hydrogen, their structures can be quite different depending on the ways hydrogen is incorporated, as was observed in the case of hydrogenated amorphous Si,[30] where $A(25)$ films have low density and a preponderance of polysilane chain segments $(SiH_2)_n$. The $A(25)$ films of a-Si-B-H alloy with high boron content which oxidize easily probably have a polymeric-like structure of large boron-hydride fragments, because boron hydrides are known to oxidize with

considerable energy liberation,[46] while elemental boron does not oxidize appreciably at room temperature. It appears that at sufficiently high substrate temperature and negative potential, B_2H_6 and SiH_4 decompose and form highly cross-linked hydrogenated silicon-boron alloys which do not oxidize easily.

B. *C*(25), *C*(270), and *A*(270) samples

Shown in Figs. 8(a)–8(c) are the transmission spectra of *a*-Si-B-H films deposited on the cathode at 25 and 270 °C, and on the anode at 270 °C, respectively. The boron concentrations of these films can be obtained from X_g and Fig. 4. Polished crystalline silicon wafers were used as substrates because the very similar refractive indices of these substrates and of the films reduce reflection at the interface and therefore the magnitude of the interference fringes. The Si-O absorption band near 1100 cm^{-1} should be disregarded in the following because it is due to oxides associated with the substrate. The major features of the spectra can be described as follows:

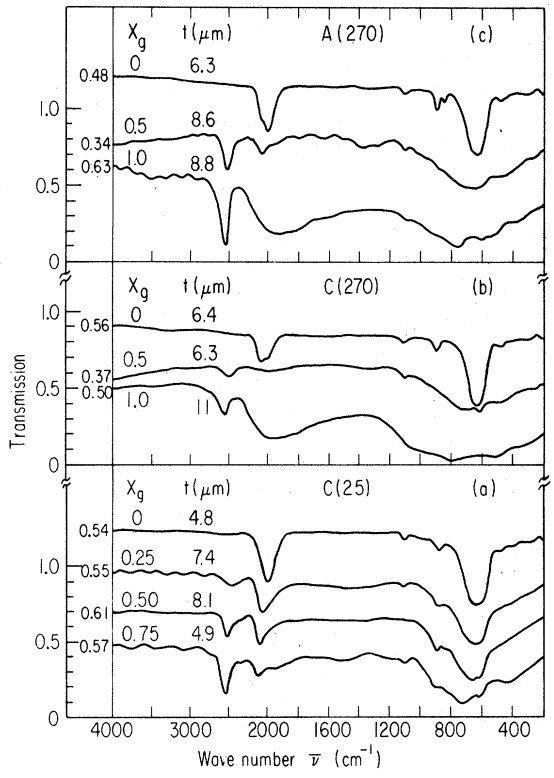

FIG. 8. Same as Fig. 6 for cathode films prepared (a) at 25 °C and (b) at 270 °C, and (c) anode films prepared at 270 °C with various X_g.

(i) The absorption band near 2560 cm^{-1} due to B-H stretching vibrations increases in intensity with increasing boron concentration, while the band near 2000–2100 cm^{-1} due to Si-H stretching vibrations decreases in intensity. It appears that hydrogen bonds about equally likely to B as it does to Si. The frequencies of these stretching vibrations are shifted by about 100 cm^{-1}, depending on the bonding environment.[22,25,30]

(ii) A broad absorption band below 1100 cm^{-1}, which overlaps the region of narrower bands observed in crystalline boron,[47] comes from B-B vibrations. As the B concentration is increased, this broad band eventually obliterates the narrower structures near 650, 840, and 890 cm^{-1}, which are due to Si-H deformation vibrations.[22,25,30] As mentioned earlier, we believe that the B-B vibrations cover a broad range of frequencies because of the formation of three-center bonds with varying bond lengths, the structural dispersion, and the breakdown of the *k*-selection rule.

(iii) Even after prolonged exposure to room air, no absorption bands corresponding to B-O near 1350 cm^{-1} or Si-O near 1050 cm^{-1} were detected except for the Si-O contribution of the substrate. These films are very stable in air, in contrast to the T_s=25 °C anode samples discussed in the previous Sec. V/A. Auger analysis revealed, however, that these samples contain a small amount of oxygen, less than 1 at.%, which appears to be too little to be detected by infrared absorption in our thin films.

(iv) A new feature was observed in the boron-rich *a*-Si-B-H alloys. This is a very broad and structureless absorption band near 1900–2000 cm^{-1} extending over 800 cm^{-1}. It is clearly seen in all the hydrogenated boron films with X_g=1, including the T_s=25 °C anode material shown in Fig. 6. It has been observed but not identified by Berezin *et al.*[43] in vacuum-deposited amorphous boron, accompanied by a strong absorption near 2560 cm^{-1} due to B-H stretching vibrations. The presence of hydrogen in vacuum-deposited amorphous boron is not so surprising because hydrogen is one of the most common impurities in all phases of boron. Although not mentioned by the authors,[43] a similar broad absorption band can be seen in the infrared-absorption spectrum of hydrogen-doped amorphous boron of Blum *et al.*[42]

This broad absorption band must come from either boron-boron bonds or boron-hydrogen bonds. Although the former cannot be ruled out, because of the possibility of second-order absorption processes involving boron modes which in first order lie below 1500 cm^{-1} according to

Berenzin *et al.*,[43] Blum *et al.*,[42] and Weber *et al.*,[48] the latter is preferred. How boron-hydrogen bonding can yield such a broad absorption band in addition to the normal boron-hydrogen stretching modes near 2560 cm^{-1} may be understood in the following way.

As mentioned earlier, boron with only three valence electrons and four orbitals is "electron deficient." As a result, three atoms can share two valence electrons to form a three-center bond. This can occur in boron hydrides where one hydrogen and two boron atoms contribute one atomic orbital each to form the lowest-energy molecular orbital.[44] This results in a B-H-B bridge bond with a hydrogen atom bridging two boron atoms. The B-H distance in symmetrical B-H-B bridge bonds is 1.33 Å, which is larger than 1.19 Å found in the normal two-center B-H terminal bonds. A diborane molecule, B_2H_6, has four B-H terminal bonds and two B-H-B bridging bonds. The stretching modes near 2600 cm^{-1} are associated with B-H terminal bonds, while an absorption band near 1984 cm^{-1} is related to the B-H-B bridge bonds in the infrared spectrum of B_2H_6.[49]

The amorphous boron-hydrogen alloy prepared at T_s=270 °C on the cathode [curve with X_g=1 in Fig. 8(b)] has a broad absorption band near 1900–2000 cm^{-1} which is much stronger than the relatively narrow band of B-H stretching modes at 2560 cm^{-1} due to the B-H terminal bonds. On the other hand, the corresponding film deposited on the anode [curve with X_g=1 in Fig. 8(c)] has similar absorption strength for both bands. The fact that the absorption strengths of these two bands are not correlated suggests that they have different origins. We therefore attribute the broad absorption band near 1900–2000 cm^{-1} to B-H-B bridge bonds. These multicenter bonds exist probably with quite different strengths in an amorphous solid because the boron atoms in B-H-B bridge bonds are under the constraints from the network. This may account for the width of the observed absorption band. The stretching vibration of the ordinary B-H terminal bonds, in contrast, should not have a broad frequency spectrum because the bond length can assume its optimal value with negligible steric hindrance.

We conclude that hydrogen can be bonded to boron as a bridging hydrogen or as a terminal hydrogen. The relative abundances of these two different bonding sites depend on T_s, the substrate potential, as well as on the plasma conditions. The hydrogenated boron film prepared on the anode at T_s=25 °C (X_g=1 curve in Fig. 6) has predominantly B-H terminal bonds in polymeric boron-hydride fragments, while those prepared at T_s=270 °C [X_g=1 curve in Figs. 8(b) and 8(c)] have an abundance of B-H-B bridge bonds in a highly cross-linked amorphous network of hydrogenated boron, with more B-H-B bridge bonds in C(270) films than in A(270) films.

Si-B bonds cause infrared absorption near 1400 cm^{-1}.[50] Very weak absorption of this kind may be seen in X_g=0.25 and 0.5 samples in Fig. 8(a), and X_g=0.5 samples in Figs. 8(b) and 8(c). There is no doubt that Si-B bonds exist in these a-Si-B-H alloys. In fact, the optical gap indicates local ordering corresponding to SiB_4 and SiB_6, as will be discussed later.

VI. OPTICAL-ABSORPTION EDGE

The optical-absorption curve $\alpha(h\nu)$ of amorphous semiconductors[51] is described in the high-absorption region ($\alpha \geq 10^4$ cm^{-1}) by

$$\alpha = B(h\nu - E_0)^2/h\nu, \quad h\nu \geq E_0 . \tag{3}$$

This relation is obtained from the assumption that the density of valence- and conduction-band states depends on energy as $N(E) \propto E^{1/2}$, and that all optical interband transitions conserving energy are allowed in amorphous semiconductors. An optical gap E_0 is defined as the intercept of the $(\alpha h\nu)^{1/2}$ vs $h\nu$ curve.

In the intermediate absorption range ($1 < \alpha < 10^4$ cm^{-1}), the absorption usually depends exponentially on photon energy as

$$\alpha(h\nu) = \alpha_0 \exp(\gamma h\nu) , \tag{4}$$

with a slope γ having values between 12 and 20 eV^{-1}. At even lower absorption constants ($\alpha < 1$ cm^{-1}), one often finds a weak and preparation-sensitive absorption tail extending to lower photon energies.

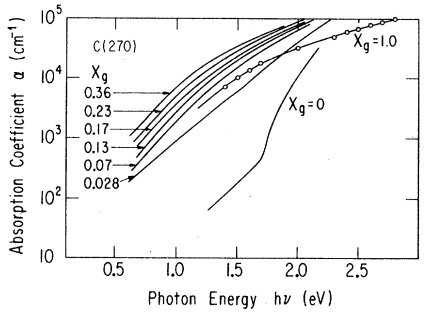

FIG. 9. Optical-absorption edge of cathode films prepared at 270 °C with X_g=0, 0.028, 0.07, 0.13, 0.17, 0.23, 0.36, and 1, respectively.

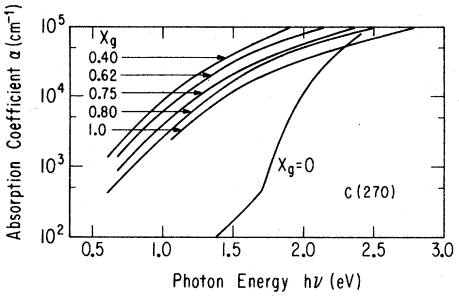

FIG. 10. Optical-absorption edge of cathode films prepared at 270 °C with $X_g = 0$, 0.40, 0.62, 0.75, 0.80, and 1, respectively.

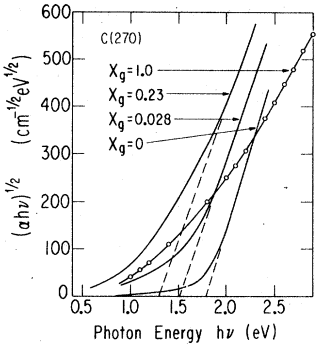

FIG. 12. Plots of $(\alpha h\nu)^{1/2}$ against photon energy of cathode films prepared at 270 °C with $X_g = 0$, 0.028, 0.23, and 1, respectively.

The glow-discharge hydrogenated silicon films were found[30] to obey Eq. (3) with an optical gap E_0 lying between 1.6 and 1.85 eV, depending on the substrate potential and the deposition temperature. These large values, as compared to 1.2–1.5 eV of sputtered or evaporated a-Si, come from the substantial hydrogen content of these films and the fact that Si-H bonds are stronger than Si-Si bonds. The constant B of Eq. (3) was found[30] to be about 6×10^5 eV^{-1} cm^{-1}, in close agreement with the values for other amorphous semiconductors.[52] In contrast to most other amorphous semiconductors there is a large preparation-sensitive absorption tail in these glow-discharge silicon films, which is illustrated by a curve labeled $X_g = 0$ in Fig. 9. This tail starts already at a values of order 10^3 cm^{-1} and obscures the exponential absorption, if present, described by Eq. (4). Such a large absorption tail below the gap energy is quite surprising because these films have much fewer localized gap states than evaporated or sputtered a-Si, which were found to have very sharp absorption edges.[53]

Incorporation of boron into these films greatly enhances the low energy absorption tail as shown in Figs. 9 and 10 for $C(270)$ samples and Fig. 11 for $A(270)$ samples. At the same time this tail appears to become an intrinsic property of the hydrogenated Si-B alloy and ceases to depend on the preparation conditions. At very high boron concentrations (see, for instance, the $X_g = 1.0$ curve in Fig. 9), one can no longer separate the tail from the part attributed to interband absorption.

This is more clearly seen in Fig. 12, which shows a plot of $(\alpha h\nu)^{1/2}$ against $h\nu$ for a few films of Fig. 9. The $X_g = 0$ curve shows a straight line portion which is described by Eq. (3) with $B = 6\times10^5$ eV^{-1} cm^{-1}. The same interpretations seem justified for $X_g = 0.028$. The $X_g = 0.23$ curve is a borderline case and requires trust in the constancy of the B value for distinguishing interband

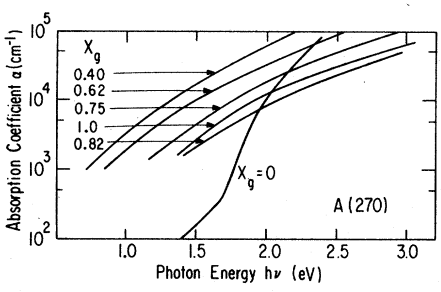

FIG. 11. Same as Fig. 10 for anode films.

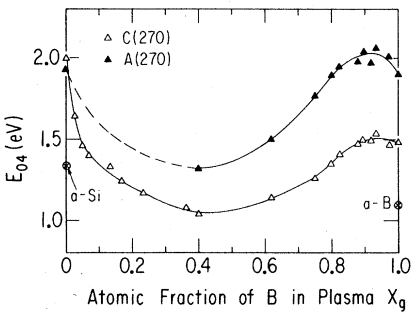

FIG. 13. Optical gap E_{04}, which is the photon energy at which $\alpha = 10^4$ cm^{-1} of films prepared at 270 °C as a function of X_g. The values 1.34 eV for sputtered a-Si (Ref. 54) and 1.1 eV for evaporated a-B (Ref. 55) are marked.

from tail absorption and for finding an intercept E_0. For larger X_g values the $(\alpha h\nu)^{1/2}$ curves continue to bend upwards with increasing photon energy in the range investigated without attaining the steepness of the low X_g curves. We are thus unable to determine E_0 by using Eq. (3) in the conventional manner or to define the onset of optical transitions from extended valence-band states to extended conduction-band states. It seems as if in films containing large boron concentrations there no longer is a sharp drop in the density of states near the mobility edges. The density of states appears to decrease smoothly into the pseudogap. This probably comes from the spread of bond distance in the three-center bonding of boron as a result of the constraint of the lattice.

Nevertheless, one can see from Fig. 9 that the absorption curves shift to lower photon energies as X_g is increased from zero to 0.36. In order to describe this shift we plot in Fig. 13 the photon energy E_{04} at which $\alpha = 10^4$ cm^{-1} as a function of X_g. One finds that E_{04} first decreases, it reaches a broad minimum near $X_g = 0.4$, and then rises again at higher boron concentrations. There is a maximum near $X_g = 0.9$. This composition corresponds quite closely to SiB_4 and SiB_6, which are the only compound compositions in the phase diagram of Si-B binary alloys. This maximum of E_{04} suggests local chemical ordering in the amorphous films associated with SiB_4 and/or SiB_6 structural units.

Also shown in Fig. 13 are the E_{04} values for sputtered a-Si ($E_{04} = 1.34$ eV),[54] and for evaporated a-B ($E_{04} = 1.1$ eV).[55] Both of these values are considerably lower than those of the corresponding hydrogenated films. An increase in the optical gap is always observed when alloying adds strong bonds to an amorphous semiconductor. This happens here too since the single bond energy of Si-H bond (3.3 eV) is larger than that of Si-Si bond (2.3 eV), and the average bond energy of B-H bond (4.0 eV) is larger than that of B-B bond (2.8 eV). In addition, the stronger the bonds, the larger the optical gap. An anode film with a certain boron concentration usually has a larger optical gap than the corresponding cathode film. This correlates with the fact that anode films on the boron-rich side of the a-Si-B-H alloys have considerably more hydrogen than the corresponding cathode films, as can be seen in Fig. 5.

VII. ELECTRICAL CONDUCTIVITY

The samples for the electrical conductivity measurements had coplanar electrodes of painted Aquadag[56] with a separation of 1–10 mm. The contacts were found to be Ohmic and of low resistance in the voltage range $V \leq 100$ V used. Film thickness was 0.3–2.5 μm. The samples were kept in a dry helium atmosphere during the measurements.

The effect of alloying on the dc conductivity of a-Si-B-H films in the temperature range of 80–450 K is shown in Figs. 14 and 15 for $C(270)$ samples with various X_g.

The interpretation of the conductivity curves is complicated because one deals with a continuous distribution $N(E)$ of states which at any given temperature contribute to the conduction with a mobility $\mu(E, T)$. The temperature dependence of the conductivity may be obtained from the Kubo-Greenwood formula[57]

$$\sigma = \int N(E)\, \mu(E, T) f(E, T)\, dE\,, \tag{5}$$

where $f(E, T)$ is the Fermi distribution function, provided correlation effects can be neglected. Under some circumstances the density of states $N(E)$ and/or the mobility function $\mu(E, T)$ drop sharply at a certain energy. The conductivity due to holes, for instance, can then be approximated by a sum of three components:

$$\sigma = \sigma_0 \exp[-(E_F - E_V)/kT] + \sigma_1 \exp[-(E_B + W_1)/kT] + \sigma_2 \exp[-(T_0/T)^{1/4}]\,. \tag{6}$$

The first term with $10^2 < \sigma_0 < 10^4\ \Omega^{-1}\,\text{cm}^{-1}$ corresponds to hole conduction in extended states below the valence-band mobility edge E_V. This term dominates at high temperatures. The second term

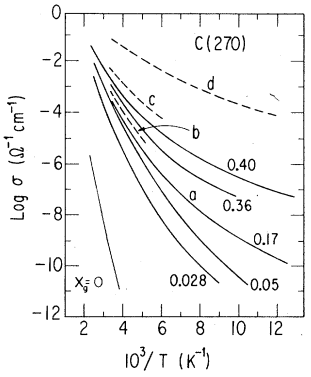

FIG. 14. Conductivity curves of cathode films deposited at 270 °C with $X_g = 0$, 0.028, 0.05, 0.17, 0.36, and 0.40, respectively. Dashed curves b, c, and d represent sample a after annealing for 30 min at 275, 470, and 570 °C, respectively.

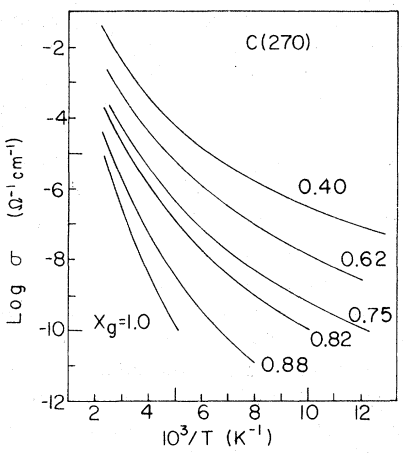

FIG. 15. Same as Fig. 14 for X_g =0.40, 0.62, 0.75, 0.82, 0.88, and 1, respectively.

describes thermally activated hopping (with an activation energy W_1) in localized states between E_V and the drop of $N(E)$ at an energy E_B. The value of σ_1 is several orders of magnitude smaller than σ_0. The last term is Mott's variable range hopping conduction[58] in states around the Fermi energy E_F, which is expected to dominate at low temperatures.

We find that the conductivity curves shown in Figs. 14 and 15 cannot be described by Eq. (6). The slopes of these Arrhenius plots decrease gradually as the temperature is lowered. Conduction in extended states dominates only for the compositions $0 < X_g < 0.4$ and for these only between $300 < T < 500$ K. Evidence for this is the fact that straight-line extrapolations of the high-temperature positions of these curves yield intercepts between 10^2 and 10^4 Ω^{-1}cm^{-1} which are acceptable values for σ_0. None of these curves, except curve labeled *d*, which will be discussed later, follow Mott's variable range hopping expression at the lowest temperature, which is 78 K.

This suggests that the density of states $N(E)$ of these alloys decreases quite gradually into the pseudogap. This conclusion agrees with our earlier observation that the optical absorption decreases unusually slowly with decreasing photon energy. As a consequence, the maximum contribution to the integral of Eq. (5) moves gradually from E_V at the highest temperatures toward E_F as the temperature is lowered. The Fermi level itself depends on temperature as discussed by Redfield,[59] because it lies in a region of changing density of states.

Figures 14 and 15 show that the conductivity first increases rapidly with boron concentration, then more slowly. It reaches a maximum near X_g=0.4 and then decreases as X_g is increased further. The conductivity curves of *A*(270) films are not shown here because they are very similar and follow the same trends as these cathode films.

Although some of the boron-rich films have not yet quite reached the region of mobility edge conduction at high temperatures, we have plotted ΔE obtained from the high-temperature slope of the conductivity curves as a function of X_g in Fig. 16. There we compare ΔE with E_{04}, which is taken as a measure of the optical gap. Despite the admitted errors in both quantities, one may conclude that ΔE is considerably smaller than one half of the optical gap except for the boron-free *a*-Si-H. This means that the Fermi level is close to one band. Thermopower measurements show that holes are the dominant carriers.[60]

Normally one would expect that boron doped with silicon should be *n*-type, while silicon doped with boron is *p*-type. If this were so, then somewhere in the *a*-Si-B-H system a change in the sign of the thermopower should occur. This is not observed. Dietz and Hermann[61] found that crystalline boron has a positive thermopower, even if it is doped with silicon or carbon. They concluded that *p*-type conductivity is characteristic of boron, in agreement with our results on Si-B alloys.

It is quite surprising that the Fermi level is close to the valence band throughout the alloy region. If B and Si preserve their normal valencies and satisfy their bonds, then E_F should be near the gap center. There appears to be a large concentration of native defects which act as acceptors and thus move E_F close to the valence band. We tested whether these defects can be

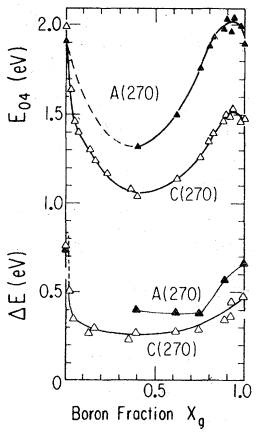

FIG. 16. Optical gap E_{04} and electrical activation energy ΔE of films prepared at 270 °C as a function of X_g.

removed by annealing. The dashed curves labeled *b*, *c*, and *d* in Fig. 14 show the result of annealing sample *a*, which has $X_g=0.17$. In contrast to the behavior of most other amorphous semiconductors, one finds that the conductivity increases with annealing and that E_F moves even closer toward the valence band. Curve *d* of Fig. 14 may be fitted by the variable range hopping term, the last term of Eq. (6) with $T_0=4\times10^7$ K. Using the relation

$$T_0=16\alpha^3/N(E_F)k \tag{7}$$

derived by Ambegoakar *et al.*,[62] one obtains $N(E_F)=4.6\times10^{18}$ cm^{-3}eV^{-1} if one uses a wave-function decay length $\alpha^{-1}=10$ Å. Not too much weight, however, should be given to this value of $N(E_F)$, because the wave-function decay length is really not known except for the fact that the width of the infrared absorption bands indicates short correlation length. The wave-function decay length can be a factor of 2 off, which would vary $N(E_F)$ by an order of magnitude either way.

Annealing may have removed gap states which counteracted the effect of the intrinsic acceptors in these alloys. In order to test this hypothesis we compare in Fig. 17 the conductivity curves of films deposited at $T_s=25$ and 270 °C. The Fermi energy is much closer to the gap center in the low-temperature films. The same behavior was found in a *a*-Si-H film lightly doped with boron or phosphorus. The doping efficiency is always larger in high T_s films. We conclude therefore that the films in the alloy range contain an appreciable concentration of acceptors. These may be boron atoms in tetrahedral coordination.

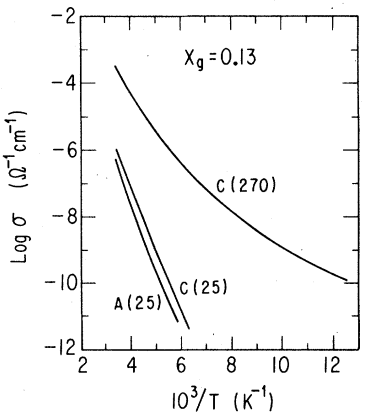

FIG. 17. Conductivity curves of cathode films prepared at 25 and 270 °C, and an anode film prepared at 25 °C, respectively, for $X_g=0.13$.

The effect of annealing on the conductivity of plasma deposited Si (Ref. 27) and Si-B alloy films is more complicated than argued above. Hydrogen effuses at these temperatures and the reconstruction and healing of the large number of potential dangling bonds left behind by the effused hydrogen is incomplete and should create new defects. The conductivity of undoped glow-discharge *a*-Si-H also increases with annealing.

Figure 16 shows that anode films deposited at 270 °C have a larger value of E_{04} and of ΔE and a correspondingly lower conductivity than cathode films deposited at the same T_s. We can think of two possible explanations: the cathode films may contain more defects because they are bombarded by argon ions during deposition, or their mobility gap is smaller because they contain less hydrogen than the anode films at a given X_g.

Hardly any photoconductivity was observed in films belonging to the alloy regime. We now wish to compare the properties of our glow-discharge deposited *a*-B-H films with those of evaporated *a*-B. Berezin *et al.*[43] reported that the conductivity of evaporated *a*-B is activated at high temperatures with $\Delta E=0.65$ eV, $\sigma_0=10^4$ Ω^{-1}cm^{-1}, and $\sigma=3\times10^{-5}$ Ω^{-1}cm^{-1} at 300 K. At low temperatures they find variable range hopping. Our *a*-B-H films deposited at $T_s=270$ °C have at the cathode $\Delta E=0.47$ eV, $\sigma_0=10$ Ω^{-1}cm^{-1}, and $\sigma_{300}=8\times10^{-8}$ Ω^{-1}cm^{-1} and at the anode $\Delta E=0.66$ eV, $\sigma_0=10^{-1}$ Ω^{-1}cm^{-1}, and $\sigma_{300}=5\times10^{-11}$ Ω^{-1}cm^{-1}. As in the case of *a*-Si, hydrogenation of amorphous boron increases the gap and greatly decreases the conductivity.

VIII. ELECTRON-SPIN RESONANCE

Figures 18 and 19 show the spin density N_s, *g* value, and peak-to-peak linewidth ΔH_{pp} of the *a*-Si-B-H films prepared at $T_s=270$ °C as a function of X_g measured by electron-spin-resonance (ESR) experiment. The observation can be summarized as follows: (i) The spin density of the *a*-Si-B alloys ($X_g\neq0$) is $N_s=1-9\times10^{18}$ cm^{-3}, essentially independent of the alloy composition, the substrate bias, and perhaps even the substrate temperature.[63] (ii) One ESR line was observed at each composition of the *a*-Si-B-H alloys. The line shape is between Loretzian and Gaussian. With increasing boron concentration, the linewidth increases from 7 G for *a*-Si-H to 35–40 G for *a*-B-H, while the *g* value decreases from 2.0062 ± 0.0005 at $X_g=0.23$ to 2.0005 ± 0.0003 for *a*-B-H.

Amorphous Si, unlike chalcogenide glasses, has a network which is overconstrained. As a re-

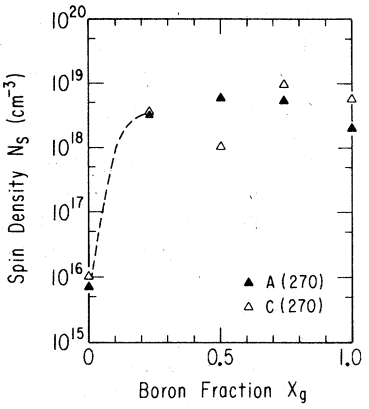

FIG. 18. Spin density of films deposited at 270 °C as a function of X_g.

sult, evaporated or sputtered a-Si usually has a large number of unpaired spins of the order of 10^{20} cm^{-3}.[64] Hydrogenated a-Si-H prepared at low T_s still has about $N_s = 5 \times 10^{19}$ cm^{-3},[27] whereas the spin density is lowered by nearly four orders of magnitude when the a-Si-H is prepared at $200 < T_s < 400$ °C.[27,64] This is because the incorporation of 10–30-at.% hydrogen, which is about 100 times larger than the number of dangling bonds found in evaporated or sputtered a-Si, not only saturates the dangling bonds, but also modifies the entire network. It is surprising that N_s of the a-Si-B-H alloys is so large even if the material is deposited at $T_s = 270$ °C. The presence of boron does not seem to relax the amorphous structure, but to yield a material which is even more constrained than a-Si-H.

The fact that boron forms multicentered bonds involving both boron and hydrogen with various bond distance, as indicated by the structureless broad infrared absorption band, may provide different environments for the spin centers and give rise to a spectrum of g values, thus causing inhomogeneous broadening of the ESR absorption. This is consistent with the observation of a large linewidth which grows with increasing boron concentration. Hyperfine interaction between electron and boron nuclei, which have nuclear magnetic moments, may also contribute to the broadening.

Hydrogenation in general seems to produce broader ESR absorption lines. This is evidenced by the larger linewidth of 35–40 G for a-B-H, as compared to 12–25 G for a-B prepared by vapor-phase decomposition[65] or electron-beam evaporation,[66] and 6–8 G for a-Si-H[64] as compared to 4–6 G for a-Si.[64] Again we believe that the inhomogeneous broadening is increased by the variety of local defect environments.

It is interesting to note that while only one ESR line is observed at each composition of the a-Si-B-H alloy, Knights *et al.*[24] found both a narrow line of $\Delta H_{pp} \sim 7$–8 G and a broad line of $\Delta H_{pp} \sim 20$ G in the lightly boron-doped a-Si-H. The former is due to a defect associated with Si, whereas the latter is probably related to the presence of boron in an environment of silicon atoms. The observation of two ESR lines in the doping regime is understandable when there are two kinds of paramagnetic centers having somewhat different g values. As the concentrations of boron and silicon become comparable in the alloy regime, the narrow ESR line due to a defect associated with Si vanishes, because the presence of substantial amount of boron greatly modifies the chemical environment of silicon. As a result, only one line is observed in the alloys; spins average over silicon and boron atoms surrounding the defects. Similar behavior was also observed in a-Si-Ge alloys.[67]

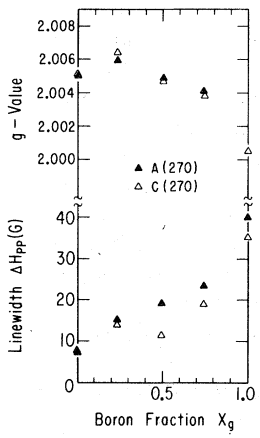

FIG. 19. g-value and peak-to-peak linewidth of ESR signals of samples prepared at 270 °C as a function of X_g.

SUMMARY AND CONCLUSIONS

Amorphous semiconducting Si-B alloys can be prepared through the whole binary system by plasma decomposition of silane-diborane mixtures. These alloys contain between 10- and 45-at.% hydrogen which is bonded in the material in various ways, depending on the temperature and the potential of the substrate with respect to the plasma.

These amorphous alloys differ from chalcogenide glasses and from group IV amorphous semiconductors in several aspects.

(i) The density of states of the valence band

and presumably also of the conduction band have tails of localized states which extend quite far into the pseudogap. Evidence for this is obtained from the following two points.

(ii) The optical-absorption coefficient α rises very gradually with increasing photon energy in the range of interband absorption. For the boron-rich alloys it is not possible to separate optical transition involving localized tail states and transition between extended band states.

(iii) The conductivity curves on a log σ vs $1/T$ plot are bending continuously between 77 and 450 K without showing distinct exponential sections or Mott's variable range hopping behavior $\sigma \propto \exp[-(T_0/T)^{1/4}]$. The conduction process changes gradually from conduction by holes in extended states at the highest temperatures to thermally assisted hopping in a gradually decreasing tail of localized states at low temperatures.

(iv) The Fermi level is near the gap center at the two ends of the binary system, a-Si-H and a-B-H. It moves close to the valence-band mobility edge for alloy compositions. This indicates self-doping with acceptors which may be boron atoms in tetrahedral coordination.

(v) There are between 10^{18} and 10^{19} cm^{-3} unpaired spins even if the alloys are plasma deposited on substrates held at 270 °C. The spin concentration of boron-free a-Si-H deposited at this temperature is as low as 10^{16} cm^{-3}.

The high spin density suggests that the structure of these hydrogenated Si-B alloys is overconstrained and does not easily allow the satisfaction of all valence bonds. This is somewhat surprising in view of the fact that boron is an electron-deficient element which can be found in various bonding arrangements, including both two-center and three-center bonds. Moreover, hydrogen forms terminal as well as bridging bonds and thus should help in reducing the chance of finding unsatisfied bonds which contribute a spin signal. The spin resonance line is inhomogeneously broadened to a width of 35–40 G in boron-rich alloys on account of the variety of bonding environments which exist in these alloys.

The variety of bonds which include among others three-center bridge bonds involving boron and hydrogen and three-center covalent bonds involving boron together with the overconstraintness of the structure yield a spectrum of bond lengths and strengths. These manifest themselves in several broad infrared absorption bands and, we surmise, in the large band tails of localized states, which in turn cause the anomalous behavior of the optical absorption and electrical conductivity.

ACKNOWLEDGMENTS

The author wishes to thank Dr. B. Grung and Prof. G. Wehner of the University of Minnesota, and D. E. Busch of the Argonne National Laboratory for performing the Auger spectroscopic analysis, and Dr. J. Ito of the University of Chicago for performing the atomic absorption spectroscopic analysis. The help of D. Dennison, P. Gaczi, P. Persans, M. Tanielian, and M. A. Vesaghi in many phases of this work is gratefully acknowledged. Most of all, the author is deeply indebted to her thesis advisor, Prof. H. Fritzsche, for his guidance, inspiration, and encouragement. This work was supported in part by NSF Grant DMR77-11683 and the Materials Research Laboratory Program of the NSF at The University of Chicago, and was submitted to the Department of Physics, The University of Chicago, in partial fulfillment of the requirement for the Ph.D. degree.

---

*Present address: Xerox Palo Alto Research Center, Palo Alto, Calif. 94304.

[1]W. E. Spear and P. G. LeComber, Solid State Commun. 17, 1193 (1975).

[2]W. E. Spear and P. G. LeComber, Philos. Mag. 33, 935 (1976).

[3]W. E. Spear, *Proceedings of the Fifth International Conference on Amorphous and Liquid Semiconductors*, edited by J. Stuke and W. Brenig (Taylor & Francis, London, 1974), p. 1.

[4]A. Madan, P. G. LeComber, and W. E. Spear, J. Non-Cryst. Solids 20, 239 (1976).

[5]J. C. Knights, AIP Conf. Proc. 31, 296 (1976).

[6]J. C. Knights, Philos. Mag. 34, 663 (1976).

[7] W. E. Spear and P. G. LeComber, *Proceedings of the Seventh International Conference on Amorphous and Liquid Semiconductors*, edited by W. E. Spear (Center for Industrial Consultancy and Liaison, University of Edinburgh, 1977), p. 309.

[8]W. E. Spear, R. J. Loveland, and A. Al-Sharbaty, J. Non-Cryst. Solids 15, 410 (1974).

[9]R. J. Loveland, W. E. Spear, and A. Al-Sharbaty, J. Non-Cryst. Solids 13, 55 (1973).

[10] D. A. Anderson and W. E. Spear, Philos. Mag. 36, 695 (1977).

[11]P. J. Zanzucchi, C. R. Wronski, and D. E. Carlson, J. Appl. Phys. 48, 5227 (1977).

[12]P. G. LeComber, A. Madan, and W. E. Spear, J. Non-Cryst. Solids 11, 219 (1972).

[13] A. R. Moore, Appl. Phys. Lett. 31, 762 (1977).

[14]D. Engemann and R. Fischer, Phys. Status Solidi B 79, 195 (1977).

[15]J. I. Pankove and D. E. Carlson, same as Ref. 7, p. 402.
[16]M. H. Brodsky, J. J. Cuomo, and F. Evangelist, same as Ref. 7, p. 397.
[17]W. E. Spear, P. G. LeComber, S. Kinmond, and M. H. Brodsky, Appl. Phys. Lett. 28, 105 (1976).
[18]D. E. Carlson and C. R. Wronski, Appl. Phys. Lett. 28, 671 (1976).
[19]C. R. Wronski, D. E. Carlson, and R. E. Daniel, Appl. Phys. Lett. 29, 602 (1976).
[20]H. Fritzsche, same as Ref. 7, p. 3; C. C. Tsai, H. Fritzsche, M. H. Tanielian, P. J. Gaczi, P. D. Persans, and M. A. Vesaghi, *ibid.*, p. 339.
[21]M. H. Brodsky, Thin Solid Films 40, L23 (1977); M. H. Brodsky, Thin Solid Films (to be published).
[22]M. H. Brodsky, M. Cardona, and J. J. Cuomo, Phys. Rev. B 16, 3556 (1977).
[23]W. Rehm. R. Fischer, J. Stuke, and H. Wagner, Phys. Status Solidi B 79, 539 (1977).
[24]J. C. Knights, D. K. Biegelsen, and I. Solomon, Solid State Commun. 22, 133 (1977).
[25]J. C. Knights, G. Lucovsky, and R. J. Nemanich, Philos. Mag. (to be published).
[26]R. A. Street, J. C. Knights, and D. K. Biegelsen, Phys. Rev. B 18, 1880 (1978).
[27]H. Fritzsche, C. C. Tsai, and P. Persans, Solid State Tech. 21, 55 (1978).
[28]H. Fritzsche, M. Tanielian, C. C. Tsai, and E. Symbalisty, Appl. Phys. Lett. 33, 353 (1978).
[29]H. Fritzsche, M. Tanielian, C. C. Tsai, and P. J. Gaczi, J. Appl. Phys. (to be published).
[30]C. C. Tsai and H. Fritzsche (unpublished).
[31]D. A. Anderson, Philos. Mag. 35, 17 (1977).
[32]D. A. Anderson and W. E. Spear, Philos. Mag. 35, 1 (1977).
[33]J. C. Knights and R. A. Lujan, J. Appl. Phys. 49, 1291 (1978).
[34]A. Triska, D. Dennison, and H. Fritzsche, Bull. APS 20, 392 (1975).
[35]M. H. Brodsky, M. A. Frisch, J. F. Ziegler, and W. A. Lanford, Appl. Phys. Lett. 30, 561 (1977).
[36]R. C. Chittick, J. H. Alexander, and H. F. Sterling, J. Electrochem. Soc. 116, 77 (1969).
[37]Thallium bromoiodide, Harshaw Chemical Co., Solon, Ohio.
[38]The Auger spectroscopic analysis was performed by B. Grung and G. Wehner of the University of Minnesota, and D. E. Busch of the Argonne National Laboratory.
[39]The atomic absorption spectroscopic analysis was performed by J. Ito of the University of Chicago.
[40]L. E. Davis, N. C. MacDonald., P. W. Palmberg, G. E. Riach, and R. E. Weber, *Handbook of Auger Electron Spectroscopy*, 2nd ed. (Physical Electronics Industries, Minnesota, 1972).
[41]The infrared transmission spectra were measured with a Perkin-Elmer Model 283 double-beam infrared spectrometer.
[42]N. A. Blum, C. Feldman, and F. G. Satkiewicz, Phys. Status Solidi A 41, 481 (1977).
[43]A. A. Berezin, O. A. Golikova, M. M. Kazanin, T. Khomidov, D. N. Mirlin, A. V. Petrov, A. S. Umarov, and V. K. Zaitsev, J. Non-Cryst. Solids 16, 237 (1974).
[44]The incorporation of three-center bonds associated with boron in amorphous semiconductors was first pointed out by S. R. Ovshinsky, same as Ref. 7, p. 519; S. R. Ovshinsky and D. Adler, Contemp. Phys. 19, 109 (1978); E. L. Muetherties, *The Chemistry of Boron and Its Compounds* (Wiley, New York, 1967).
[45]W. Zimmerman III, A. M. Murphy, and C. Feldman, Appl. Phys. Lett. 10, 71 (1967).
[46]Boron hydrides have been considered for use as rocket fuel.
[47]O. A. Golikova, I. A. Drakin, V. K. Zaitsev, M. M. Kazanin, D. N. Mirlin, I. V. Nelson, E. N. Tkalenko, and T. Khomidov, *Proceedings of the Fourth International Conference on Boron*, Vol. 2, *Tbilisi, 1972* (Metsniereba, Tbilisi, 1974).
[48]W. Weber and M. F. Thorpe, J. Phys. Chem. Solids 36, 967 (1975).
[49]W. C. Price, J. Chem. Phys. 16, 894 (1948).
[50]B_6Si *infrared transmission spectrum* (Sadtler Research Laboratories, Inc., Philadelphia, Penn., 1972).
[51]J. Tauc, *Amorphous and Liquid Semiconductors*, edited by J. Tauc (Plenum, New York, 1974), p. 159.
[52]N. F. Mott and E. A. Davis, *Electronic Processes in Non-Crystalline Materials* (Clarendon, Oxford, 1971), p. 251.
[53]M. L. Theye, *Optical Properties of Solids: New Developments*, edited by B. O. Seraphin (North-Holland, Amsterdam, 1976), p. 353.
[54]M. H. Brodsky, R. S. Title, K. Weiser, and G. D. Pettit, Phys. Rev. B 1, 2632 (1970).
[55]K. Moorjani and C. Feldman, Solid State Commun. 6, 473 (1968).
[56]Aquadag is colloidal graphite in water from Acheson Colloids Co., Port Huron, Michigan.
[57]R. Kubo, Can. J. Phys. 34, 1274 (1956).
[58]See p. 41 of Ref. 52.
[59]D. Redfield, Phys. Rev. Lett. 27, 730 (1971).
[60]P. Persans (unpublished).
[61]W. Dietz and H. Hermann, *Boron, Vol. 2, Preparation, Properties, and Applications*, edited by G. K. Gaule (Plenum, New York, 1965), p. 107.
[62]V. Ambegoakar, B. I. Halperin, and J. S. Langer, Phys. Rev. B 4, 2612 (1971).
[63]An anode a-Si-B-H film deposited at $T_S = 25\,^{\circ}C$ also has $N_S \sim 2\times10^{18}\,cm^{-3}$, although not too much weight should be placed on this measurement because of the high oxidation rate of the A (25) alloys with $X_g \neq 0$. However, it would be coincident that all factors cancel out such that the hygroscopic and oxidized alloys have the same spin concentration as the stable samples.
[64]J. Stuke, same as Ref. 7, p. 406, and references therein.
[65]J. J. Koulmann, G. Gewinner, L. Kubler, and A. Jaéglé, Phys. Status Solidi B 68, K43, (1975); G. Gewinner, L. Kubler, J. J. Koulmann, and A. Jaéglé, Phys. Status Solidi B 70, 595 (1975).
[66]C. Feldman, H. K. Charles, Jr., F. G. Satkiewicz, and J. Bohandy, J. of the Less-Common Metals 47, 141 (1976).
[67]M. Kumeda, Y. Jinno, and T. Shimizu, Phys. Status Solidi B 81, K71 (1977).